PCCP

PAPER

View Article Online
View Journal | View Issue

Cite this: *Phys. Chem. Chem. Phys.*, 2024, **26**, 24498

Achieving 9% EQE in light-emitting electrochemical cells *via* a TADF-sensitized fluorescence strategy†

Zeyang Zhou,‡[ab] Qingda Chang,‡[ab] Rui Chen,[ab] Pengfei Jin,[ab] Baipeng Yin,*[a] Chuang Zhang*[a] and Jiannian Yao[ac]

Light-emitting electrochemical cells (LECs) are appealing for cost-effective, large-area emission applications; however, their luminescence efficiency is significantly limited by exciton annihilation caused by high concentration polarons. Here, we present thermally activated delayed fluorescence (TADF) sensitized fluorescence LECs (TSF-LECs) that achieve a record 9% EQE. The TADF sensitizers with rapid reverse intersystem crossing (RISC) rates can effectively convert triplet excitons to singlet excitons in LECs, thereby establishing a more efficient overall energy transfer pathway. Importantly, magneto-electroluminescence measurements indicate that the additional RISC route in TSF-LECs significantly suppresses the annihilation of triplet excitons and thus reduces exciton loss under high concentration polaron conditions. Compared to LECs without a sensitizer, TSF-LECs exhibit improved EQE and luminance, extended operational lifetimes, and suppressed efficiency roll-off. A flexible display prototype based on TSF-LECs was further fabricated, capable of stably displaying high-brightness preset patterns for extended periods. The exploration of the exciton dynamics in high concentration polaron environments offers valuable insights for future developments in high-efficiency LEC technology.

Received 15th July 2024,
Accepted 4th September 2024

DOI: 10.1039/d4cp02801e

rsc.li/pccp

Introduction

Light-emitting electrochemical cells (LECs) are emerging as a promising emission technology with broad application prospects in solid-state lighting,[1–8] wearable illuminated devices[9] and health-monitoring sensors.[10] Distinct from commercial emission technologies such as organic light emitting diodes (OLEDs) and light emitting diodes (LEDs), LECs are simple three-layer devices consisting of an active layer containing emissive molecules and mobile ions sandwiched between the anode and cathode. When a voltage is applied between the electrodes, ion migration within the active layer results in the formation of stable electrochemical doping regions at the anode (p-doped) and cathode (n-doped), enabling charge injection regardless of the electrode work function.[11,12] This allows the use of air-stable electrode materials in LECs, reducing the need for rigorous encapsulation.[13–16] Moreover, charge injection and ion migration adaptively expand the doped regions over time to ensure that charge recombination and light emission occur in the intrinsic region, thereby improving the tolerance of LECs to the thickness and roughness of active layers.[17,18] Unfortunately, high concentration polarons stabilized in the doped region can cause intense exciton annihilation, leading to a low external quantum efficiency (EQE) and efficiency roll-off in LECs.[19–23] Thus, it is necessary to develop a strategy to enhance exciton utilization under high concentration polarons for device efficiency optimization, which may be an effective way to advance LECs towards practical applications.

Using thermally activated delayed fluorescence (TADF) materials with high photoluminescence quantum yield (PLQY) as emitters is an effective method to improve the utilization of excitons for their ability to convert optically dark triplet excitons to optically bright singlet excitons.[24–28] Despite the huge success of this strategy in OLEDs, the efficiency optimization in TADF-LECs is still below expectations. This is because TADF emitters with high radiative transition rates typically have lower reverse intersystem crossing (RISC) rates, making it difficult to efficiently convert triplet excitons exposed to high concentration polarons in LECs.[29,30] The TADF-sensitized fluorescence (TSF) strategy is a further extension of the TADF approach, integrating TADF sensitizers to address the challenge of balancing the rates of RISC and radiative transition. A TADF sensitizer with a rapid

[a] *Key Laboratory of Photochemistry, Beijing National Laboratory for Molecular Sciences, Institute of Chemistry, Chinese Academy of Sciences, Beijing 100190, China. E-mail: yinbaipeng@iccas.ac.cn, zhangc@iccas.ac.cn*
[b] *University of Chinese, Academy of Sciences, Beijing 100049, China*
[c] *Institute of Molecular Engineering Plus, Fuzhou University, Fuzhou 350108, China*
† Electronic supplementary information (ESI) available. See DOI: https://doi.org/10.1039/d4cp02801e
‡ These authors contributed equally.

RISC rate can more efficiently convert triplet excitons into singlet excitons, which are then transferred to TADF emitters with high radiative transition rates for efficient emission.[31–34] This synergistic effect minimizes exciton quenching and improves the overall energy utilization efficiency. Nevertheless, given the structural difference between LECs and OLEDs, high performance LECs *via* the TSF mechanism still require further validation.

In this work, 10,10′-(4,4′-sulfonylbis(4,1-phenylene))bis(9,9-dimethyl-9,10-dihydroacridine) (DMAC-DPS) was chosen as a TADF sensitizer to prepare TSF-LECs, with poly(*N*-vinyl carbazole) (PVK)/1,3-bis(2-(4-*tert*-butylphenyl)-1,3,4-oxadiazo-5-yl)benzene (OXD-7) as the mix-host and 3,4,5,6-tetrakis(3,6-di-*t*-butylcarbazol-9-yl)-1,2-dicyanobenzene (4CzPN-*t*Bu) as the TADF emitter. The introduction of TADF sensitizers facilitates the optimization of the overall energy transfer efficiency in LECs, as their rapid RISC can efficiently convert triplet excitons into singlet excitons. Magneto-electroluminescence (MEL) techniques and transient-EL measurement further reveal that the additional RISC route can effectively reduce exciton–polaron annihilation and maximize exciton utilization in LECs in the presence of high concentration polarons. Consequently, TSF-LECs exhibited excellent emission performance with an EQE of 9% and a device LT_{50} lifetime of more than 20 hours, thereby establishing a new EQE benchmark for TADF LECs.[2,35] Based on the potential of TSF-LECs for high efficiency, high stability, and ease of processing, we fabricated a flexible display prototype capable of stably displaying preset patterns with high brightness over extended periods.

Experimental methods

Device fabrication and characterization

ITO substrates were cleaned carefully using toluene, acetone, and *tert*-butanol for 20 min, respectively, by using an ultrasonic bath and then dried at 110 °C before being treated with oxygen plasma. PEDOT:PSS solutions were spin-coated onto ITO at 4000 rpm for 45 s and annealed in air at 150 °C for 30 min. The substrates were then transferred into a glove box ($O_2 < 1$ ppm, $H_2O < 1$ ppm) for the remaining fabrication steps. The active material solutions composed of PVK/OXD-7, DMAC, 4CzPN-*t*Bu and $THABF_4$ were prepared by dissolving in chlorobenzene (organic luminescent molecule's total concentration is maintained at 20 mg mL^{-1}). In the fabrication of the LECs, the active-material solutions were then spin-coated (2000 rpm, 60 s) on top of the ITO/PEDOT:PSS layer and annealed at 70 °C for 30 min. To complete the devices, an Al cathode (100 nm, deposited at 1.0 Å s^{-1}) was deposited using thermal vacuum evaporation with a pressure of $< 5 \times 10^{-5}$ Pa.

Photophysical characterization

The absorption spectra were measured using a Hitachi UH4150 at normal incidence, and the fluorescence spectra were measured using a Hitachi F-7000. The transient PL decay characteristics were measured using a Quantaurus-Tau C11367-35 at an excitation wavelength of 360 nm. The absolute PL quantum yield was determined using a Hamamatsu C11347 coupled with an integrating sphere.

MEL measurements

For MEL measurements, LECs were transferred to a vacuum chamber of a cryostat (Oxford OptistatDry BLV) that was placed in an electromagnet (EastChangjing, EM4) with a magnetic field of up to 200 mT. The LECs were operated at forward bias above turn-on voltages powered using a Keithley 2450 Source Meter, and the EL emission was monitored with a silicon detector (Thorlab SM05PD2A). The MEL was defined as: $MEL(B) = [EL(B) - EL(0)]/EL(0) \times 100\%$ measured at a constant bias. The external magnetic field was swept at a rate of 10 mT s^{-1} in one direction and back for several cycles to improve the S/N ratio of MEL(B). The sensitivity of the MEL measurements was typically 0.05%, and the statistics on multiple LECs were given as error bars in the main text.

Measurement of transient-EL and device performances

A Keithley 2400 and a spectroradiometer (Photo Research, PR788) were used to test the current–voltage and the luminance properties, respectively. The transient–EL curves were measured using a 50 μs electrical pulse at 10 V bias using a signal generator Tektronix AFG1062. Data of transient EL were recorded by the TCSPC method using a Single-Photon Counting Module (excelitas SPCM-AQRH-14) and a time-to-digital converter (qutools quTAG), respectively. The external quantum efficiencies were calculated according to luminance, EL spectrum, and current density of all devices (assuming a Lambertian distribution).

Results and discussion

Fig. 1a illustrates the device structure of our target TSF-LECs, which consists of an active layer containing host materials, organic emissive materials and mobile ions, sandwiched between an indium tin oxide (ITO) anode and an aluminium (Al) cathode. In this structure, the p-type semiconductor poly(*N*-vinyl carbazole) (PVK) and the n-type semiconductor 1,3-bis(2-(4-*tert*-butylphenyl)-1,3,4-oxadiazo-5-yl)benzene (OXD-7) were chosen as mixed host materials, and tetrahexylammonium tetrafluoroborate ($THABF_4$) was chosen as the electrolyte (Fig. S1, ESI†). 3,4,5,6-Tetrakis(3,6-di-*t*-butylcarbazol-9-yl)-1,2-dicyanobenzene (4CzPN-*t*Bu) is a sophisticatedly designed TADF material that utilizes non-radiative triplet excitons through RISC and features large intramolecular steric hindrance to suppress non-radiative transitions, resulting in a high photoluminescence quantum yield (PLQY). Consequently, it was chosen as a terminal emitter to be doped into the host materials (Fig. 1b, left). When a voltage is applied between the electrodes, 25% of the optically bright singlet excitons and 75% of the optically dark triplet excitons are formed on the host and then transferred to the TADF emitter through energy transfer. The triplet excitons can be converted into the singlet excitons through the RISC process of TADF emitters with high PLQY and finally participate in the effective radiative process (blue arrows in Fig. 1a). However, TADF emitters with a high PLQY, ***i.e.*** a high radiative transition rate, usually possess a lower RISC rate. Therefore, in the presence of high concentrations of polarons, the probability of triplet excitons interacting with polarons increases,

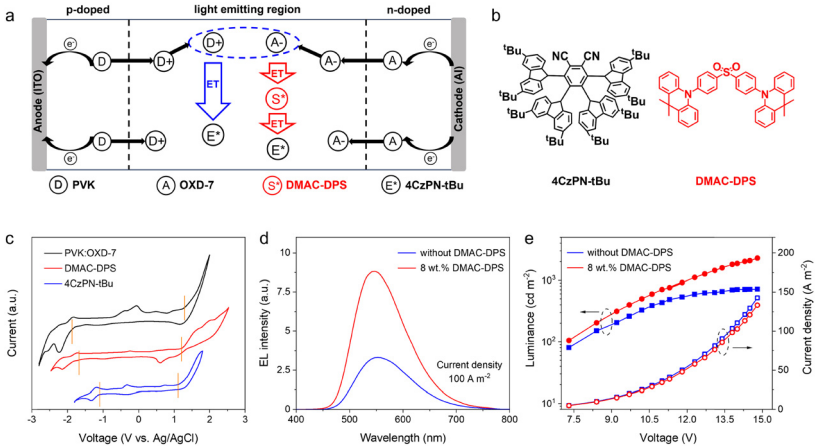

Fig. 1 (a) Schematics of the operation mechanism of LECs after the formation of the electric double layers (EDLs), p-doped, n-doped, and intrinsic zones. The red and blue arrows represent the energy transfer processes with and without a sensitizer, respectively. (b) Chemical structure of emitter 4CzPN-*t*Bu and sensitizer DMAC-DPS. (c) Cyclic voltammograms of mix-host PVK:OXD-7, sensitizer DMAC-DPS, and emitter 4CzPN-*t*Bu. (d) EL spectrum measured from LECs with and without DMAC-DPS. (e) Current density (A m^{-2})–voltage (V)–luminance (cd m^{-2}) curve of LECs with and without DMAC-DPS.

leading to loss by triplet-polaron annihilation (TPA). To address this issue, TADF materials with a high RISC rate can be introduced as sensitizers into LECs to facilitate the rapid conversion of triplet excitons into singlet excitons, achieving efficient exciton utilization (red arrows in Fig. 1a). 10,10′-(4,4′-Sulfonylbis(4,1-phenylene))bis(9,9-dimethyl-9,10-dihydroacridine) (DMAC-DPS) consists of two DMAC moieties as intramolecular donors and one DPS moiety as an intramolecular acceptor, and is capable of forming a twisted intramolecular D–A–D structure (Fig. 1b, right). This structure endows its excited state with charge-transfer characteristics, resulting in a minimal singlet–triplet energy gap (ΔE_{ST}), which in turn grants it an exceptionally rapid RISC rate, making it an ideal sensitizer in TSF-LECs. Electron–hole analysis of the sensitizer also reveals a transition from the DMAC moiety to the DPS moiety, indicating strong charge transfer excitation properties (Fig. S2, ESI†).

Optical spectroscopy is performed to investigate the energy transfer pathway in TSF-LECs. As shown in Fig. S3 (ESI†), the emission spectrum of the DMAC-DPS/PVK:OXD-7 doped films is consistent with that of the pristine DMAC-DPS film, indicating the effective energy transfer from the host to the sensitizer. Moreover, the large overlap between the emission spectrum of DMAC-DPS and the absorption spectrum of 4CzPN-*t*Bu implies that the Förster resonance energy transfer (FRET) between them can be efficient (Fig. S4, ESI†). We then measured the redox potentials of each component within TSF-LECs using cyclic voltammetry to calculate their band gaps, as shown in Fig. 1c. The results revealed a sequential band gap gradient from the host to the sensitizer and finally to the emitter, indicating that the incorporation of the DMAC-DPS sensitizer successfully established a spontaneous host–sensitizer–emitter energy transfer pathway in LECs. Fig. 1d illustrates the electroluminescence (EL) spectra of LECs with 8 wt% and without the DMAC-DPS sensitizer, with similar spectral shapes indicating that the emission originates from the 4CzPN-*t*Bu emitter in both cases. However, we observed that the EL intensity of LECs with a sensitizer increases significantly. Then, the current density (*J*)–voltage (*V*)–luminance (*L*) curves of LECs with 8 wt% and without the DMAC-DPS sensitizer were measured, revealing that the luminance of LECs with the sensitizer was also significantly improved, with a maximum increase of more than threefold (Fig. 1e). The nearly identical current density at the same voltage indicates that the incorporation of the TADF sensitizer can improve device performance by optimizing the efficiency of the entire energy transfer pathway rather than affecting the electrical properties of LECs.

To reveal the operational mechanism of the TSF strategy in LECs, it is essential to investigate the interplay between the sensitizer and emitter within the ternary system in the presence of mobile ions. Therefore, we prepared film samples with varying sensitizer-to-emitter ratios for systematic photophysical testing. As shown in Fig. S5 (ESI†), with a fixed sensitizer concentration of 10 wt% in the host, the photoluminescence (PL) intensity of the DMAC-DPS sensitizer at ~460 nm gradually decreases and eventually disappears as the emitter concentration increases from 0 to 2 wt%. This suggested that complete energy transfer from the sensitizer to the emitter occurred in the ternary system. The energy transfer rate constant k_{ET} between the emitter and sensitizer can be fitted from the transient PL decay curves for these doped films (Fig. S6 and S7, ESI†). The results show that k_{ET} gradually increases and ultimately exceeds sensitizer's radiation transition rate k_r as the emitter concentration increases from 0 to 2 wt%, which leads to efficient energy transfer from the sensitizer to the emitter. The emitter concentration was then fixed at 2 wt%, and as the sensitizer concentration increased from 0 to 10 wt%, the PL spectra of almost all the doped films showed only the emission of the 4CzPN-*t*Bu emitter (Fig. S8, ESI†). Moreover, the emission from the sensitizer in these doped films vanishes after 60 ns, which is more rapid than the PL decay time scale of the pristine DMAC-DPS film (Fig. 2a). These results indicate that the sensitizer can efficiently transfer energy to the emitter in a short period of time.

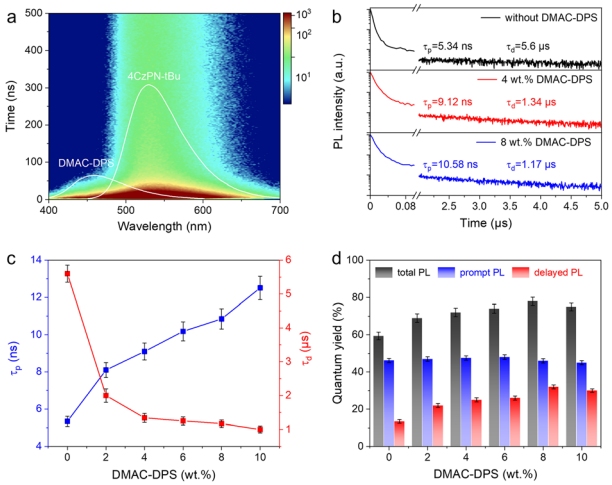

Fig. 2 (a) Time-resolved photoluminescence (PL) spectrum of a 2 wt% 4CzPN-*t*Bu doped with an 8 wt% DMAC-DPS blend film, where white lines depict the spectral profiles of DMAC-DPS and 4CzPN-*t*Bu. (b) Transient photoluminescence (PL) spectra of 2 wt% 4CzPN-*t*Bu doped with a DMAC-DPS at concentrations of 0, 4, and 8 wt% blend film, measured at 500 nm. (c) Prompt lifetime and delayed lifetime of the blend film doped with DMAC-DPS at various concentrations (0, 2, 4, 6, 8, and 10 wt%). (d) Prompt and delayed quantum yield of the blend film doped with DMAC-DPS at various concentrations (0, 2, 4, 6, 8, and 10 wt%).

Transient PL decay measurements on the 4CzPN-*t*Bu emitter in doped films were further performed to investigate the kinetic process of the sensitizer-to-emitter energy transfer. As shown in Fig. 2b, the transient PL decay measured at ~500 nm can be decomposed into a short-lived component (τ_p) and a long-lived component (τ_d), corresponding to the prompt and delayed fluorescence of the 4CzPN-*t*Bu emitter, respectively. As the sensitizer concentration increases from 0 to 10 wt%, τ_d decreases from 5.60 μs to 1.0 μs, while τ_p increases from 5.34 ns to 12.5 ns (Fig. 2c). The decrease in τ_d implies that more triplet excitons are collected by the RISC process of the sensitizer than by that of the emitter since the sensitizer possesses a more rapid RISC rate. An increase in τ_p also implies the presence of an additional energy transfer pathway from the singlet of the sensitizer to the singlet of the emitter, which is consistent with the decrease in τ_d. Subsequently, the PLQYs of doped films with sensitizer concentrations from 0–10 wt% were measured, as shown in Fig. 2d. Compared to that of films without a sensitizer, the PLQY of doped films with a sensitizer significantly increased, reaching 78.0% at a sensitizer concentration of 8 wt%. According to Fig. S9 (ESI†), the PLQY consists of contributions from both the short-lived component and the long-lived component. It can be clearly seen that the increase in the total PLQY is mainly attributed to the increase in the PLQY of the long-lived component. This further demonstrates that the incorporation of the TADF sensitizer can improve the overall energy utilization efficiency by converting triplet excitons back into singlet excitons.

Based on the above experimental results, we established a possible mechanism for exciton management in TSF-LECs, as illustrated in Fig. 3a. Under electrical excitation, 75% of the triplet excitons and 25% of the singlet excitons are generated on the mix-host, with the energy of the triplet excitons subsequently being transferred to the sensitizer. DMAC-DPS has a ΔE_{ST} of 274 meV, which is lower than that (360 meV) of its counterpart, and thus exhibits a faster RISC rate (Fig. S2, ESI†).[36–38] Given that the DMAC-DPS sensitizer has a higher RISC rate, it can effectively convert the energy of triplet excitons into singlet excitons, and then rely on rapid FRET between the sensitizer and the emitter to transfer the energy to the emitter. Thus, sensitizer doping introduces a faster RISC pathway into the system, reducing the population of triplet excitons and preventing exciton annihilation, ultimately improving the efficiency of LECs. To validate this TSF-LEC strategy, we extracted the lifetime of the electro-exciton by measuring the transient EL spectra of LECs with different sensitizer concentrations. The

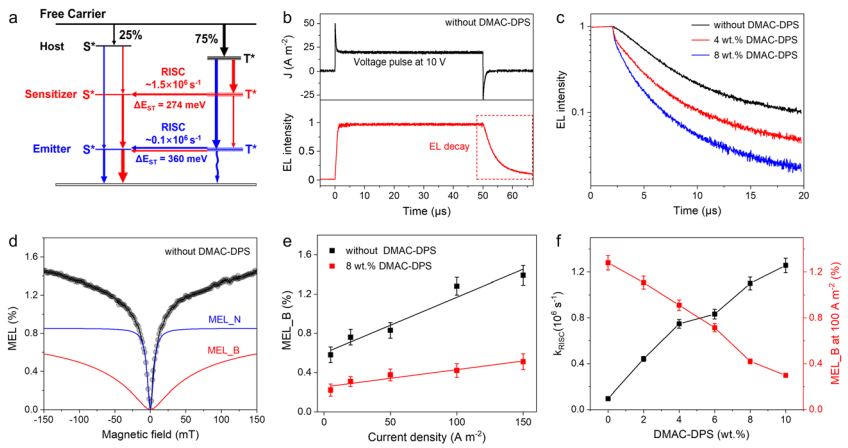

Fig. 3 (a) Diagram of the exciton process in the TSF-LECs. (b) The current and EL response of LECs without a sensitizer under a pulse at 10 V. (c) EL decay curves of LECs with 2 wt% 4CzPN-*t*Bu, doped with DMAC-DPS at concentrations of 0, 4, and 8 wt%. (d) Magneto-electroluminescence profile of LECs without DMAC-DPS under constant 30 A m^{-2}, decomposed into low-field (MEL_N) and high-field (MEL_B) effects. (e) Relationship between current density and the amplitudes of the MEL_B component in LECs with and without DMAC-DPS. (f) The relationship between the RISC rate (k_{RISC}) and the amplitudes of MEL_B with varying concentrations of DMAC-DPS.

excitation conditions were 10 V electrical pulse, 50 μs pulse width, and 1 kHz frequency. As shown in Fig. 3b, the current of LECs reverses to the maximum current after the pulse voltage is turned off and then slowly returns to zero, which can be attributed to the capacitance effect. This current recovery process follows an exponential attenuation, and the RC time of LECs can be obtained by exponential fitting of this curve. The fitted RC time (<1 μs) is much shorter than the EL lifetime of LECs, making its impact on electroluminescence negligible (Fig. S10, ESI†). Therefore, the EL lifetime can be considered the lifetime of the electro-exciton. Clearly, the LECs with a sensitizer exhibit a shorter EL lifetime than LECs without a sensitizer (Fig. 3c). Furthermore, as the sensitizer concentration increases, the EL lifetime of LECs further decreases, indicating the effective conversion of triplet excitons by the sensitizer's rapid RISC. In contrast, devices without a sensitizer show a slower decline in EL decay curves between 2 and 5 μs. The absence of DMAC-DPS reduces the RISC rate, slowing down triplet exciton consumption and sustaining electron–hole recombination after the pulse ends, resulting in a less steep EL decay. To investigate the impact of the TSF strategy on the exciton annihilation effect in LECs, we measured the magneto-electroluminescence (MEL) response of the devices, as the dynamic processes of triplet excitons are sensitive to changes in the external magnetic field.[39–42] As shown in Fig. 3d, the MEL curve of LECs increases and gradually saturates with the increasing magnetic field. The MEL magnitude at a given magnetic field B is defined as MEL(B) = [EL(B) − EL(0)]/EL(0) × 100%, where EL(0) is the EL intensity measured at zero field. By Lorentzian and non-Lorentzian fitting, the MEL curve of LECs can be decomposed into two components: MEL_N, which corresponds to the low-field effect, and MEL_B, which corresponds to the high-field effect. According to previous reports, the MEL_B component originates from TPA, and its magnitude is positively correlated with the strength of TPA.[43,44] Therefore, we extracted the MEL_B magnitude from LECs with and without sensitizers in the current density range of 0–150 A m^{-2} to evaluate their TPA process, as shown in Fig. 3e. It is evident that LECs with a sensitizer exhibit lower MEL_B magnitude, indicating that the exciton quenching process caused by high concentrations of polarons in LECs is significantly suppressed. This conclusion is further confirmed by the dependence of the RISC rates and MEL_B magnitude (at 100 A m^{-2}) in LECs with different sensitizer concentrations. As shown in Fig. 3f, as the RISC rate increases, the MEL_B value, *i.e.*, the strength of TPA, in LECs decreases accordingly.

The device efficiency of TSF-LECs with PVK (52.2 wt%)/OXD-7 (34.8 wt%)/$THABF_4$(3 wt%)/DMAC-DPS (8 wt%)/4CzPN-*t*Bu (2 wt%) was further evaluated. As shown by the EQE–current density characteristics in Fig. 4a, TSF-LECs exhibited a maximum EQE of 9%, which is 1.5 times greater than that of LECs without a sensitizer. To the best of our knowledge, this value is the highest reported for TADF LECs to date. In addition, a suppressed efficiency roll-off was observed for TSF-LECs, with the EQE decreasing by ∼10% and ∼15% when the current density was increased to 50 A m^{-2} and 100 A m^{-2}, respectively. In contrast, the EQE of LECs without a sensitizer decreased by ∼33% and ∼60%

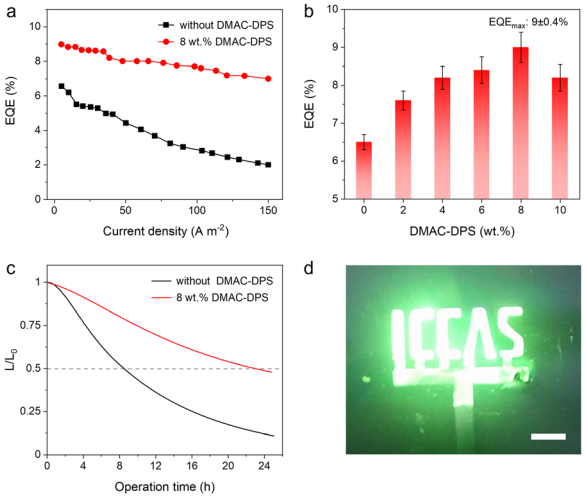

Fig. 4 (a) EQE–current density characteristics of LECs with 8 wt% and without DMAC-DPS. (b) EQE values measured at 100 cd m^{-2} and different sensitizer concentrations. (c) Normalized luminance as a function of operational time with an initial of L_0 = 100 cd m^{-2} at constant current with 8 wt% and without DMAC-DPS. (d) Image of TSF-LECs with a pattern of the abbreviation of "ICCAS", and the scale bar represents 0.5 cm.

at a current density of 50 A m^{-2} and 100 A m^{-2}, respectively. This phenomenon is consistent with the variation trend of MEL_B against current density shown in Fig. 3e, which can be attributed to the fact that, in the presence of the sensitizer, the TPA process is less sensitive to the increased polaron concentration. As shown in Fig. 4b, the EQE_{max} of LECs exhibited an increasing trend with increasing sensitizer doping concentration, which is consistent with the observed changes in MEL_B with varying DMAC-DPS concentrations (Fig. 3f). This result implied that within a certain concentration range, increasing the concentration of the sensitizer can effectively reduce TPA, thereby enhancing the EQE. Furthermore, the device lifetimes were evaluated with a luminance of 100 cd m^{-2}, as shown in Fig. 4c. Compared to LECs without a sensitizer, which possess an LT_{50} of only 8 hours (LT_{50} represents the time required for the luminance to decay to 50% of the initial luminance at a constant operating current density), TSF-LECs demonstrated an improved lifetime of more than 20 hours. Based on the potential of TSF-LECs for high efficiency, high stability, and ease of processing, we fabricated a flexible display prototype, as shown in Fig. 4d. In ambient air, a simple spin-coating process was used to deposit the mixed active materials onto a pre-patterned PET/ITO substrate, resulting in a high-brightness TSF-LEC device with dimensions of 5 × 5 cm. This device was driven by a constant current of 25 A m^{-2}, and stably displayed the "ICCAS" pattern for 10 hours. These results demonstrate the advantages of the TSF strategy in improving the performance of LECs and represent an encouraging step forward toward the commercialization of LECs.

Conclusions

In conclusion, our work demonstrates the significant potential of integrating TADF sensitizers into LECs to enhance their

performance and achieve a record EQE of 9%. By incorporating TADF sensitizer DMAC-DPS into a mix-host of PVK/OXD-7 and using 4CzPN-*t*Bu as the TADF emitter, we can harness both the sensitizer's rapid RISC rate for efficient triplet exciton conversion and the emitter's rapid radiative transition rate for effective emission. Steady state and transient optical spectroscopy reveals that the TADF sensitizer introduces a novel energy transfer pathway, significantly improving exciton and energy utilization efficiency. EL and MEL demonstrate that in the presence of a high concentration of polarons, the new energy transfer pathway can effectively reduce TPA and exciton loss, thereby boosting device efficiency. This work sets a new EQE benchmark for TADF LECs and validates the TSF strategy's potential in high polaron environments, offering valuable insights for future developments in high-efficiency LEC technology.

Author contributions

J. Y., C. Z. and B. Y. supervised the project. Z. Z. prepared the blend samples and fabricated the LEC devices. Z. Z. and Q. C. carried out the optical spectroscopy measurements. H. W. carried out the electroluminescence and magneto-electroluminescence measurements. Z. Z., R. C., P. J. and B. Y. analysed the data. Q. C., B. Y. and Z. Z. wrote the draft. All authors discussed and contributed to the manuscript preparation.

Data availability

The authors confirm that the data supporting the findings of this study are available within the article and its ESI.†

Conflicts of interest

There are no conflicts to declare.

Acknowledgements

This work was financially supported by the Ministry of Science and Technology of China (No. 2018YFA0704802 and 2020YFA0714603), the National Natural Science Foundation of China (No. 22090021 and 52303262), and the CAS "Strategic Priority Research Program B" (No. XDB0520302).

Notes and references

1 Q. Pei, G. Yu, C. Zhang, Y. Yang and A. J. Heeger, Polymer Light-Emitting Electrochemical Cells, *Science*, 1995, **269**, 1086–1088.
2 P. Lundberg, Y. Tsuchiya, E. M. Lindh, S. Tang, C. Adachi and L. Edman, Thermally activated delayed fluorescence with 7% external quantum efficiency from a light-emitting electrochemical cell, *Nat. Commun.*, 2019, **10**, 5307.
3 Z. Q. Li, Y. D. Wang, J. Y. Shao, Z. Zhou, Z. L. Gong, C. Zhang, J. Yao and Y.-W. Zhong, Electrically Amplified Circularly Polarized Luminescence by a Chiral Anion Strategy, *Angew. Chem., Int. Ed.*, 2023, **62**, e202302160.
4 S. Tang, Z. Wang, Y. Xu, H. Ma, J. Wang, C. Larsen, D. Dang, E. Wang and L. Edman, Aggregation-Induced Emission by Molecular Design: A Route to High-Performance Light-Emitting Electrochemical Cells, *Angew. Chem., Int. Ed.*, 2023, **62**, e202302874.
5 A. Jouaiti, L. Ballerini, H.-L. Shen, R. Viel, F. Polo, N. Kyritsakas, S. Haacke, Y.-T. Huang, C.-W. Lu, C. Gourlaouen, H.-C. Su and M. Mauro, Binuclear Copper(I) Complexes for Near-Infrared Light-Emitting Electrochemical Cells, *Angew. Chem., Int. Ed.*, 2023, **62**, e202305569.
6 G. Giobbio, L. M. Cavinato, E. Fresta, A. Montrieul, G. Umuhire Mahoro, J.-F. Lohier, J.-L. Renaud, M. Linares, S. Gaillard and R. D. Costa, Design Rule Hidden from The Eye in S/N-Bridged Ancillary Ligands for Copper(I) Complexes Applied to Light-Emitting Electrochemical Cells, *Adv. Funct. Mater.*, 2023, **33**, 2304668.
7 S. Tang, J. M. dos Santos, J. Ràfols-Ribé, J. Wang, E. Zysman-Colman and L. Edman, Introducing MR-TADF Emitters into Light-Emitting Electrochemical Cells for Narrowband and Efficient Emission, *Adv. Funct. Mater.*, 2023, **33**, 2306170.
8 S. Watanabe, L. M. Cavinato, V. Calvi, R. van Rijn, R. D. Costa and K. Oyaizu, Polarizable H-Bond Concept in Aromatic Poly(thiourea)s: Unprecedented High Refractive Index, Transmittance, and Degradability at Force to Enhance Lighting Efficiency, *Adv. Funct. Mater.*, 2024, 2404433.
9 J. Shen, C. Chui and X. Tao, Luminous fabric devices for wearable low-level light therapy, *Biomed. Opt. Express*, 2013, **4**, 2925–2937.
10 T. Yokota, P. Zalar, M. Kaltenbrunner, H. Jinno, N. Matsuhisa, H. Kitanosako, Y. Tachibana, W. Yukita, M. Koizumi and T. Someya, Ultraflexible organic photonic skin, *Sci. Adv.*, 2016, **2**, e1501856.
11 M. J. Jafari, J. O. Pedersen, S. Barhemat and T. Ederth, In Situ Surface-Enhanced Raman Spectroscopy on Organic Mixed Ionic-Electronic Conductors: Tracking Dynamic Doping in Light-Emitting Electrochemical Cells, *ACS Appl. Mater. Interfaces*, 2024, **16**, 28938–28948.
12 K. Yasuji, T. Sakanoue, F. Yonekawa and K. Kanemoto, Visualizing electroluminescence process in light-emitting electrochemical cells, *Nat. Commun.*, 2023, **14**, 992.
13 E. Auroux, A. Sandström, C. Larsen, E. Zäll, P. Lundberg, T. Wågberg and L. Edman, Evidence and Effects of Ion Transfer at Active-Material/Electrode Interfaces in Solution-Fabricated Light-Emitting Electrochemical Cells, *Adv. Electron. Mater.*, 2021, **7**, 2100253.
14 L. M. Cavinato, G. Millán, J. Fernández-Cestau, E. Fresta, E. Lalinde, J. R. Berenguer and R. D. Costa, Versatile Biogenic Electrolytes for Highly Performing and Self-Stable Light-Emitting Electrochemical Cells, *Adv. Funct. Mater.*, 2022, **32**, 2201975.
15 C.-M. Wang, Y. M. Su, T. A. Shih, G. Y. Chen, Y. Z. Chen, C. W. Lu, I. S. Yu, Z. P. Yang and H. C. Su, Achieving highly saturated single-color and high color-rendering-index white light-emitting electrochemical cells by CsPbX3 perovskite

color conversion layers, *J. Mater. Chem. C*, 2018, **6**, 12808–12813.

16 J. Xu, A. Sandström, E. M. Lindh, W. Yang, S. Tang and L. Edman, Challenging Conventional Wisdom: Finding High-Performance Electrodes for Light-Emitting Electrochemical Cells, *ACS Appl. Mater. Interfaces*, 2018, **10**, 33380–33389.

17 E. Auroux, A. Sandström, C. Larsen, P. Lundberg, T. Wågberg and L. Edman, Solution-based fabrication of the top electrode in light-emitting electrochemical cells, *Org. Electron.*, 2020, **84**, 105812.

18 K. Schlingman, Y. Chen, R. S. Carmichael and T. B. Carmichael, 25 Years of Light-Emitting Electrochemical Cells: A Flexible and Stretchable Perspective, *Adv. Mater.*, 2021, **33**, 2006863.

19 J.-H. Shin, N. D. Robinson, S. Xiao and L. Edman, Polymer Light-Emitting Electrochemical Cells: Doping Concentration, Emission-Zone Position, and Turn-On Time, *Adv. Funct. Mater.*, 2007, **17**, 1807–1813.

20 J. D. Slinker, J. A. DeFranco, M. J. Jaquith, W. R. Silveira, Y.-W. Zhong, J. M. Moran-Mirabal, H. G. Craighead, H. D. Abruña, J. A. Marohn and G. G. Malliaras, Direct measurement of the electric-field distribution in a light-emitting electrochemical cell, *Nat. Mater.*, 2007, **6**, 894–899.

21 H. Iwakiri, H. Watanabe and Y. Noguchi, Investigating Bulk-to-Interface Doping Relaxation in Light-Emitting Electrochemical Cells via Displacement Current Measurements, *ACS Appl. Electron. Mater.*, 2021, **3**, 2355–2361.

22 M. Diethelm, A. Devižis, W. H. Hu, T. Zhang, R. Furrer, C. Vael, S. Jenatsch, F. Nüesch and R. Hany, Traps for Electrons and Holes Limit the Efficiency and Durability of Polymer Light-Emitting Electrochemical Cells, *Adv. Funct. Mater.*, 2022, **32**, 2203643.

23 S. van Reenen, R. A. J. Janssen and M. Kemerink, Fundamental Tradeoff between Emission Intensity and Efficiency in Light-Emitting Electrochemical Cells, *Adv. Funct. Mater.*, 2015, **25**, 3066–3073.

24 X. Tang, L. S. Cui, H. C. Li, A. J. Gillett, F. Auras, Y. K. Qu, C. Zhong, S. T. E. Jones, Z. Q. Jiang, R. H. Friend and L. S. Liao, Highly efficient luminescence from space confined charge transfer emitters, *Nat. Mater.*, 2020, **19**, 1332–1338.

25 N. B. Kotadiya, P. W. M. Blom and G.-J. A. H. Wetzelaer, Efficient and stable single-layer organic light-emitting diodes based on thermally activated delayed fluorescence, *Nat. Photonics*, 2019, **13**, 765–769.

26 Y. Xu, X. Liang, X. Zhou, P. Yuan, J. Zhou, C. Wang, B. Li, D. Hu, X. Qiao, X. Jiang, L. Liu, S. J. Su, D. Ma and Y. Ma, Highly Efficient Blue Fluorescent OLEDs Based on Upper Level Triplet–Singlet Intersystem Crossing, *Adv. Mater.*, 2019, **31**, 1807388.

27 S. Diesing, L. Zhang, E. Zysman-Colman and I. D. W. Samuel, A figure of merit for efficiency roll-off in TADF-based organic LEDs, *Nature*, 2024, **627**, 747–753.

28 J. Jiang and J. Y. Lee, Degradation mechanisms and lifetime extending strategy of phosphorescent and thermally activated delayed-fluorescence organic light-emitting diodes, *Mater. Today*, 2023, **68**, 204–233.

29 J. U. Kim, I. S. Park, C.-Y. Chan, M. Tanaka, Y. Tsuchiya, H. Nakanotani and C. Adachi, Nanosecond-time-scale delayed fluorescence molecule for deep-blue OLEDs with small efficiency rolloff, *Nat. Commun.*, 2020, **11**, 1765.

30 H. Uoyama, K. Goushi, K. Shizu, H. Nomura and C. Adachi, Highly efficient organic light-emitting diodes from delayed fluorescence, *Nature*, 2012, **492**, 234–238.

31 C.-Y. Chan, M. Tanaka, Y.-T. Lee, Y.-W. Wong, H. Nakanotani, T. Hatakeyama and C. Adachi, Stable pure-blue hyperfluorescence organic light-emitting diodes with high-efficiency and narrow emission, *Nat. Photonics*, 2021, **15**, 203–207.

32 D. Zhang, X. Song, M. Cai and L. Duan, Blocking Energy-Loss Pathways for Ideal Fluorescent Organic Light-Emitting Diodes with Thermally Activated Delayed Fluorescent Sensitizers, *Adv. Mater.*, 2018, **30**, 1705250.

33 M. Tanaka, R. Nagata, H. Nakanotani and C. Adachi, Understanding degradation of organic light-emitting diodes from magnetic field effects, *Commun. Mater.*, 2020, **1**, 1–9.

34 K. Stavrou, L. G. Franca, A. Danos and A. P. Monkman, Key requirements for ultraefficient sensitization in hyperfluorescence organic light-emitting diodes, *Nat. Photonics*, 2024, **18**, 554–561.

35 J. Ye, Y. He, K. Li, L. Liu, C. Xi, Z. Liu, Y. Ma, B. Zhang, Y. Bao, W. Wang, Y. Cheng and L. Niu, Achieving Record Efficiency and Luminance for TADF Light-Emitting Electrochemical Cells by Dopant Engineering, *ACS Appl. Mater. Interfaces*, 2022, **14**, 17698–17708.

36 T. Lu, A comprehensive electron wavefunction analysis toolbox for chemists, Multiwfn, *J. Chem. Phys.*, 2024, **161**, 082503.

37 Z. Liu, T. Lu and Q. Chen, An sp-hybridized all-carboatomic ring, cyclo[18]carbon: Electronic structure, electronic spectrum, and optical nonlinearity, *Carbon*, 2020, **165**, 461–467.

38 T. Lu and F. Chen, Multiwfn: A multifunctional wavefunction analyzer, *J. Comput. Chem.*, 2012, **33**, 580–592.

39 X. Liu, H. Popli, O. Kwon, H. Malissa, X. Pan, B. Park, B. Choi, S. Kim, E. Ehrenfreund, C. Boehme and Z. V. Vardeny, Isotope Effect in the Magneto-Optoelectronic Response of Organic Light-Emitting Diodes Based on Donor–Acceptor Exciplexes, *Adv. Mater.*, 2020, **32**, 2004421.

40 L. Guo, S. Hu, X. Gu, R. Zhang, K. Wang, W. Yan and X. Sun, Emerging Spintronic Materials and Functionalities, *Adv. Mater.*, 2024, **36**, 2301854.

41 H. Wang, J. Chen, S. Yang, H. Lu, F. Wei, Y. Wu, X. Zhao, L. Cheng, Z. Li, Y. Yi, T. Yu, S. Zhang, H. Zhu, X. Chen and Z. Xiong, Harvesting Hot Excitons for High-Efficiency OLEDs with Extremely Low-Efficiency Roll-Off *via* Utilizing the Cascade Exciton Energy Transfer from Host and Sensitizer to Emitter, *Adv. Funct. Mater.*, 2024, 2403388.

42 S. Hirata, Y. Sakai, K. Masui, H. Tanaka, S. Y. Lee, H. Nomura, N. Nakamura, M. Yasumatsu, H. Nakanotani, Q. Zhang, K. Shizu, H. Miyazaki and C. Adachi, Highly efficient blue electroluminescence based on thermally activated delayed fluorescence, *Nat. Mater.*, 2015, **14**, 330–336.

43 C. Zhao, C. Li, Y. Li, Y. Qiu and L. Duan, Understanding the operational lifetime expansion methods of thermally activated delayed fluorescence sensitized OLEDs: a combined study of charge trapping and exciton dynamics, *Mater. Chem. Front.*, 2019, **3**, 1181–1191.

44 Y. Wang, Y. Ning, F. Wu, J. Chen, X. Chen and Z. Xiong, Observation of Reverse Intersystem-Crossing From the Upper-Level Triplet to Lowest Singlet Excitons (T2 → S1) in Tetra(*t*-butyl)rubrene-Based OLEDs for Enhanced Light-Emission, *Adv. Funct. Mater.*, 2022, **32**, 2202882.